Nonlinear Dyn (2009) 57: 231–251
DOI 10.1007/s11071-008-9435-2

ORIGINAL PAPER

Two-to-one internal resonance in microscanners

Mohammed F. Daqaq · Eihab M. Abdel-Rahman · Ali H. Nayfeh

Received: 12 July 2007 / Accepted: 8 September 2008 / Published online: 8 October 2008

Abstract To realize large scanning angles, torsional microscanners are normally excited at their natural frequencies. Usually, a bias DC voltage is also applied to scan around a desired nonzero tilt angle. As a result, a deep understanding of the mirror's response to a DC-shifted primary resonance excitation is imperative. Along these lines, we use the method of multiple scales to obtain a second-order nonlinear approximate analytical solution of the mirror steady-state response. We show that the response of the mirror exhibits a softening-type behavior that increases as the magnitude of the DC component increases. For a given mirror, we can also identify a DC voltage range wherein the mirror exhibits a two-to-one internal resonance between the first two modes; that is, $\omega_2 \approx 2\omega_1$. To analyze the mirror behavior within that range, we first treat the case where the excitation frequency is near the first-mode frequency; that is, $\Omega \approx \omega_1$. Then we treat the case where the excitation frequency is near the second-mode frequency; that is, $\Omega \approx \omega_2$. We analyze the stability of the response and compare the analytical results to numerical solutions obtained via long-time integration of the equations of motion. We show that, due to the internal resonance, the mirror exhibits complex dynamic behavior characterized by aperiodic responses to primary resonance excitations. This behavior results in undesirable oscillations that are detrimental to the mirror performance, namely bringing the target point in and out of focus and resulting in distorted images.

Keywords Microscanner · Nonlinear interactions · Method of multiple scales

M.F. Daqaq (✉)
Department of Mechanical Engineering, Clemson University, Clemson, SC 29634, USA
e-mail: mdaqaq@clemson.edu

E.M. Abdel-Rahman
Systems Design Engineering, University of Waterloo, Waterloo, Canada

A.H. Nayfeh
Department of Engineering Science and Mechanics, Virginia Tech, Blacksburg, VA 24061, USA

1 Introduction

The area of Micro-Opto-ElectroMechanical Systems (MOEMS) is one of the fastest growing in microsystem industry. These systems consist of two main components: an electronic component fabricated using integrated circuit (IC) technology, which provides the actuation signal, and a mechanical component usually micromachined into the silicon wafer, which represents the moving parts of the device. To realize the optical characteristics of these devices, a highly reflective surface, usually a metal film, is deposited on top of the moving components. MOEMS are utilized in many optical devices to steer, reflect, or modulate light, depending on the application at hand.

Fig. 1 A schematic of the micromirror

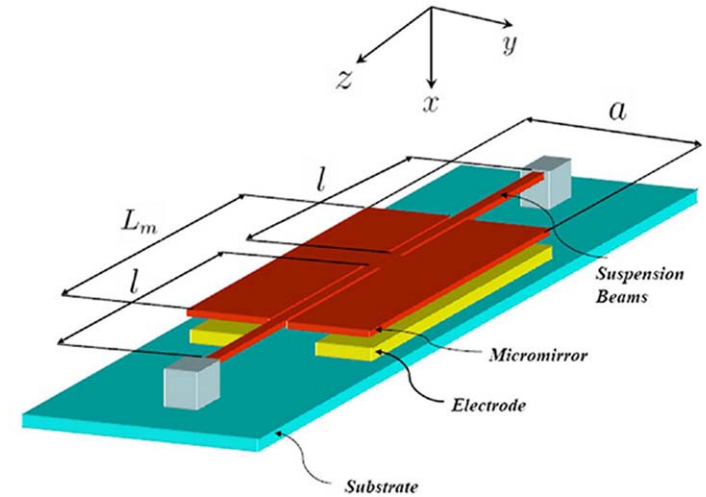

(a) Perspective view

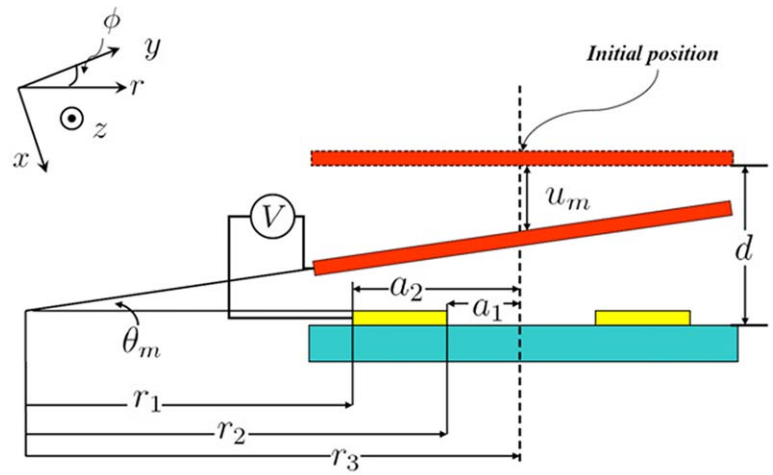

(b) Side view

Torsional micromirrors are some of the most famous and widely used MOEMS. As depicted in Fig. 1, a torsional micromirror typically consists of two identical microbeams, each beam is fixed on one side and connected to a rigid plate (the reflective surface) on the other side. Two electrodes mounted beneath the plate are used to rotate it in either direction by supplying a voltage to the corresponding electrode.

Torsional micromirrors are used in projection displays [1], switching in fiber-optic networks [2, 3], neural networks [4], phase modulating filters, optical computing [5], electrophotographic printers, and folded spectrum analyzers [6]. Additionally, the fast response of micromirrors to electric excitations made them appealing substitutes for traditional scanning technologies. Specifically, torsional micromirrors have been successfully implemented in resonant optical microscanners [7]. In scanning applications, the micromirror is usually excited at a resonant frequency using an AC voltage component. This will help realize large scanning angles while minimizing the voltage requirements. To scan around nonzero static tilt angles, a DC bias voltage can also be applied. The action of the micromirror steers a laser beam along a sur-

face. The beam is then reflected from the surface to be collected and analyzed through a photo detector. Resonant scanning micromirrors are currently being used in a variety of applications, including laser printing, confocal microscopy, and scanning video displays.

There is a significant body of research on modeling and dynamic characterization of torsional micromirrors. Many researchers treat the micromirror as a 1-DOF lumped-mass attached to two torsional springs representing the suspension beams, and investigate the static response to predict the *pull-in* point. Osterberg [8] introduced a simple approach to analyze the static tilt angle of a torsional micromirror. Using the parallel-plate approximation to estimate the electrostatic torque and a linear spring model to estimate the torsional stiffness of the suspension beams, he developed the simplest analytical model of the mirror. Although the model is numerically efficient, the results are 20% away from experimental findings. Hornbeck [9] enhanced Osterberg's model by developing an analytical expression for the electrostatic torque based on the solution of Laplace's equation between two semi-infinite tilted plates. He numerically solved for the micromirror tilt angle at a given voltage and gradually increased the voltage until pull-in was reached. This numerical approach is extremely accurate, but requires successive numerical solutions of a complex nonlinear algebraic equation. To alleviate this shortcoming, other researchers [10–14] developed analytical methods to calculate the pull-in parameters of a 1-DOF lumped-mass torsional micromirror.

Degani and Nemirovisky [15] were the first to introduce a 2-DOF lumped-mass model that includes both torsion and bending to capture the static behavior of a torsional microactuator. Huang et al. [16] adopted this model to study the static behavior of a torsional micromirror. They derived the equations governing the response of the mirror to a DC voltage and studied the effect of electrode size and position on pull-in. They found that neglecting the bending of the suspension beams can result in more than 20% error in predicting the static tilt angles.

Most of the available dynamic models are also 1-DOF lumped-mass models [17–19]. Ataman and Urey [20] analyzed the dynamics of a resonant microscanner subjected to pure AC voltage excitations using a 1-DOF torsional lumped-mass model. Based on the solution of the Mathieu equation, they analyzed the response of the mirror and characterized its linear stability. Furthermore, for large scanning angles, they numerically analyzed the nonlinear response and observed a softening-type nonlinearity. This softening behavior was also experimentally reported by Camon and Lanaudi [21].

Zhao et al. [22] were the first to consider the coupling effect between torsion and bending in a dynamic model. They treated the mirror as a lumped mass attached to two springs. The springs represent the torsional and bending stiffness of the suspension beams. They numerically simulated the dynamic response of the micromirror to step and pure AC voltage excitations. Their numerical simulations also revealed a softening-type behavior.

To the authors' knowledge, the nonlinear dynamics of microscanners has yet to be addressed comprehensively. In this work, we utilize the method of multiple scales to analyze the nonlinear response of a micromirror subjected to combined DC and resonant AC excitations. We show that, within a range of DC voltages, a two-to-one internal resonance might be activated between the first two modes. We identify and analyze the response within this range. We show that, due to this internal resonance, the energy fed to the first (torsion) mode can be channeled to the second (bending) mode even if the bending motions are very small. The energy transfer results in undesirable oscillations detrimental to the scanner performance. If not well-understood and accounted for during the design process, these oscillations may yield aperiodic responses that will limit the operation range of the scanner to very small tilt angles.

2 Problem formulation

We consider the micromirror shown in Fig. 1. It consists of two identical microbeams of length l, width w, and thickness h. Each beam is fixed on one side and connected to a rigid rectangular plate (the mirror) on the other side. The mirror has a length L_m, width a, and thickness h_2. Beneath the micromirror there are two electrodes, each of length b and width $(a_2-a_1)/2$. The perpendicular distance between the undeformed position of the mirror and the electrodes is denoted as d. The whole microstructure is etched out of a silicon substrate that has a density ρ, the Young modulus E, and a modulus of rigidity G. The material properties and dimensions of the mirror are listed in Table 1.

The mirror is rotated in either direction by supplying a voltage $V(t)$ to the corresponding electrode. This

Table 1 Material properties and dimensions of the torsional micromirror. The parameters are typical of torsional micromirrors and are adopted after Zhao et al. [22]

Properties	
Modulus of elasticity, E[GPa]	170
Modulus of rigidity, G[GPa]	66
Density, ρ[kg/m^3]	2330
Dielectric constant of air, $\epsilon_0[F/m]$	8.85×10^{-12}
Dimensions	
Mirror width, a[μm]	100
Mirror length, L_m[μm]	100
Mirror thickness, h_2[μm]	1.50
Beam length, l[μm]	45
Beam width, w[μm]	1.55
Beam thickness, h[μm]	1.50
Electrode length, b[μm]	100
Electrode parameter, $\alpha = \frac{2a_1}{a}$	0.3
Electrode parameter, $\beta = \frac{2a_2}{a}$	1
Gap height, d[μm]	2.75

results in an electrostatic potential between the electrode and the mirror, which generates an electrostatic pressure on the surface of the mirror, and hence produces a downward electrostatic force and an electrostatic moment around the suspension axis. Consequently, the microbeams undergo simultaneous rotation $\Theta(z,t)$ and deflection $U(z,t)$. This drives the micromirror to rotate an angle $\theta_m = \Theta(l,t)$ and deflect a distance $u_m = U(l,t)$.

The mirror can be treated as a lumped mass, whereas each of the suspension beams is treated as a combined torsional and translational (bending in the x-direction) spring. Bending motions in the y-direction due to excitation asymmetries or design imperfections are assumed to be negligible. This model has been developed, verified, and shown to provide excellent representation of the mirror behavior when the frequency of excitation is close to the first two natural frequencies [22, 23]. The torsional spring has an effective stiffness $k_{11} = \frac{2GJ_b}{l}$, where

$$J_b = \frac{16w^4}{3}\left[1 - \frac{192(w/h)}{\pi^5}\sum_{n=0}^{\infty}\frac{1}{(2n+1)^5} \times \tanh\frac{(2n+1)^5}{2(w/h)}\right] \quad (1)$$

is the polar moment of inertia of the suspension beams, which accounts for cross-sectional warping effects [24]. The two microbeams have effective bending stiffness $k_{22} = \frac{24EI_{b_y}}{l^3}$, where $I_{b_y} = \frac{1}{12}wh^3$ is the area moment of inertia about the y-axis. The kinetic and potential energies of the reduced system can be written as

$$KE = \frac{1}{2}m_{11}\theta_{\rm cr}^2\dot{\theta}^2 + \frac{1}{2}m_{22}d^2\dot{u}^2, \quad (2)$$

$$PE = \frac{1}{2}k_{11}\theta_{\rm cr}^2\theta^2 + \frac{1}{2}k_{22}d^2u^2 - \frac{1}{2}CV^2 - Mgdu, \quad (3)$$

where C is the capacitance between the micromirror and the active electrode given by [16]

$$C = \frac{\epsilon_0 L_m}{\theta\theta_{\rm cr}}\ln\left[\frac{1-u-\alpha\theta}{1-u-\beta\theta}\right], \quad (4)$$

and

$$V = V_{\rm dc} + V_{\rm ac}\cos(\Omega t),$$

$$\theta = \frac{\theta_m}{\theta_{\rm cr}}, \qquad u = \frac{u_m}{d},$$

$$\theta_{\rm cr} = \arctan\left(\frac{2d}{a}\right) \approx \frac{2d}{a},$$

$$m_{11} = \frac{I_{m_{zz}}}{T^2}, \qquad m_{22} = \frac{M}{T^2},$$

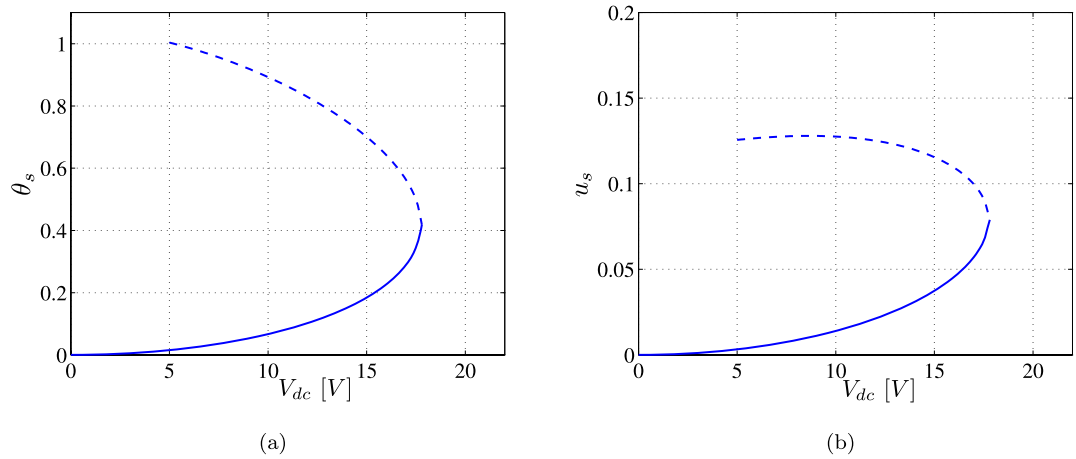

Fig. 2 Variation of the static position of the micromirror with the applied DC voltage. Dashed lines represent unstable equilibria

where $I_{m_{zz}} = \frac{1}{12}\rho a h L_m (h_2^2 + a^2)$ is the mass moment of inertia of the mirror around the z-axis, $m = \rho w h$ is the mass of the microbeam per unit length, $M = \rho h_2 L_m a$ is the mass of the mirror, V_{dc} is a direct voltage component, V_{ac} is an alternating voltage component, Ω is its frequency, and

$$T^2 = \frac{\rho w h l^2 (h^2 + w^2)}{3 G J_b} \tag{5}$$

is a time scale. We note that the capacitance has a removable singularity at zero tilt angles. To avoid computational overflow, we remove the singularity by taking the limit as θ approaches zero and obtain

$$C|_{\theta=0} = \frac{\epsilon_0 L_m}{\theta_{\text{cr}}} \frac{\beta - \alpha}{(1-u)}. \tag{6}$$

The equations of motion are given by the Euler–Lagrange equations as

$$m_{11}\ddot{\theta} + \mu_1 \dot{\theta} + k_{11}\theta = \frac{V^2}{2\theta_{\text{cr}}^2} \frac{\partial C}{\partial \theta}, \tag{7}$$

$$m_{22}\ddot{u} + \mu_2 \dot{u} + k_{22} u = \frac{V^2}{2d^2} \frac{\partial C}{\partial u} + \frac{Mg}{d}, \tag{8}$$

where $\mu_1 = \sqrt{k_{11} m_{11}}/Q$ and $\mu_2 = \sqrt{k_{22} m_{22}}/Q$ are modal damping terms and Q is the quality factor. It is worth noting that (7) and (8) are linearly and nonlinearly coupled through the electrostatic potential, hence the torsional and bending responses are both statically and dynamically coupled.

The equations representing the static response of the mirror can be obtained by setting the time variation in (7) and (8) equal to zero to obtain

$$k_{11}\theta_s = \frac{V_{\text{dc}}^2}{2\theta_{\text{cr}}^2} \frac{\partial C}{\partial \theta}\bigg|_{\theta_s, u_s} \tag{9}$$

$$k_{22} u_s = \frac{V_{\text{dc}}^2}{2d^2} \frac{\partial C}{\partial u}\bigg|_{\theta_s, u_s} + \frac{Mg}{d}. \tag{10}$$

Equations (9) and (10) are solved numerically for the equilibrium position (θ_s, u_s) corresponding to a given DC voltage V_{dc}. Figure 2(a) and (b) displays, respectively, variations of the static rotation angle and deflection of the torsional micromirror with the applied DC voltage. The pull-in parameters, which represent the upper limits of the safe operating regime of the mirror, are $V_{\text{pull-in}} \approx 17.95$ V, $\theta_{\text{pull-in}} \approx 0.399$ and $u_{\text{pull-in}} \approx 0.0264$ (nondimensional quantities). Voltage values that are beyond the pull-in point result in the mirror snapping down and colliding with the nearest electrode. See [10, 16] for more details on the static response of torsional micromirrors.

3 Nonlinear analysis

We analyze the response of the micromirror to electric excitations consisting of a DC component V_{dc} and

an AC component $V_{\rm ac}\cos(\Omega t)$. We start by expressing the response as the sum of a static part (u_s, θ_s) and a dynamic part $(u_\delta, \theta_\delta)$ as follows:

$$\begin{aligned}\theta(t) &= \theta_s + \theta_\delta(t),\\ u(t) &= u_s + u_\delta(t).\end{aligned} \tag{11}$$

Substituting (11) into (7) and (8), noting that u_s and θ_s satisfy (9) and (10), and expanding the electrostatic force and moment in Taylor series, keeping only terms up to third order in θ_δ and u_δ, we obtain

$$\begin{aligned}&m_{11}\ddot{\theta}_\delta + \mu_1\dot{\theta}_\delta + k_{11}\theta_\delta\\ &\quad= -\Gamma_1\alpha_{11}V_{\rm dc}^2 + \Gamma_1 V^2\big(\alpha_{11} + \alpha_{12}\theta_\delta + \alpha_{13}u_\delta\\ &\qquad+ \alpha_{14}\theta_\delta u_\delta + \alpha_{15}\theta_\delta^2 + \alpha_{16}u_\delta^2 + \alpha_{17}\theta_\delta u_\delta^2\\ &\qquad+ \alpha_{18}\theta_d^2 u_\delta + \alpha_{19}\theta_\delta^3 + \alpha_{110}u_\delta^3\big),\\ &m_{22}\ddot{u}_\delta + \mu_2\dot{u}_\delta + k_{22}u_\delta\\ &\quad= -\Gamma_2\alpha_{21}V_{\rm dc}^2 + \Gamma_2 V^2\big(\alpha_{21} + \alpha_{22}\theta_\delta + \alpha_{23}u_\delta\\ &\qquad+ \alpha_{24}\theta_\delta u_\delta + \alpha_{25}\theta_\delta^2 + \alpha_{26}u_\delta^2 + \alpha_{27}\theta_\delta u_\delta^2\\ &\qquad+ \alpha_{28}\theta_\delta^2 u_\delta + \alpha_{29}\theta_\delta^3 + \alpha_{210}u_\delta^3\big),\end{aligned} \tag{12}$$

where

$$\Gamma_1 = \frac{\epsilon_0 L_m}{2\theta_{\rm cr}^3}, \qquad \Gamma_2 = \frac{\epsilon_0 L_m}{2d^2\theta_{\rm cr}}, \tag{13}$$

and the α_{ij} are the coefficients resulting from the Taylor series expansions. We scale the dependent variables such that the effect of the nonlinearity balances the effects of the damping and AC excitation as

$$\begin{aligned}V &= V_{\rm dc} + \varepsilon^2 V_{\rm ac}\cos(\Omega t),\\ \mu_1 &= \varepsilon\mu_1, \qquad \mu_2 = \varepsilon\mu_2\end{aligned} \tag{14}$$

where ε is a small nondimensional bookkeeping parameter. The time dependence t is expanded in terms of multiple time scales, $T_n = \varepsilon^n t$, so that the first and second time derivatives become [25]

$$\begin{aligned}\frac{d}{dt} &= D_0 + \varepsilon D_1 + \varepsilon^2 D_2 + \cdots,\\ \frac{d^2}{dt^2} &= D_0^2 + 2\varepsilon D_0 D_1 + \varepsilon^2 D_1 + 2\varepsilon^2 D_0 D_2 + \cdots,\end{aligned} \tag{15}$$

where $D_n = \frac{\partial}{\partial T_n}$. We seek a solution of (12) in the form

$$\begin{aligned}\theta_\delta &= \varepsilon\theta_0(T_0, T_1, T_2) + \varepsilon^2\theta_1(T_0, T_1, T_2)\\ &\quad+ \varepsilon^3\theta_2(T_0, T_1, T_2) + \cdots,\\ u_\delta &= \varepsilon u_0(T_0, T_1, T_2) + \varepsilon^2 u_1(T_0, T_1, T_2)\\ &\quad+ \varepsilon^3 u_2(T_0, T_1, T_2) + \cdots.\end{aligned} \tag{16}$$

Substituting (14)–(16) into (12) and equating coefficients of like powers of ε, we obtain

$O(\varepsilon)$:

$$\begin{aligned}&m_{11}D_0^2\theta_0 + \big(k_{11} - V_{\rm dc}^2\Gamma_1\alpha_{12}\big)\theta_0 - V_{\rm dc}^2\Gamma_1\alpha_{13}u_0 = 0,\\ &m_{22}D_0^2 u_0 + \big(k_{22} - V_{\rm dc}^2\Gamma_2\alpha_{23}\big)u_0 - V_{\rm dc}^2\Gamma_2\alpha_{22}\theta_0 = 0;\end{aligned} \tag{17a}$$

$O(\varepsilon^2)$:

$$\begin{aligned}&m_{11}D_0^2\theta_1 + \big(k_{11} - V_{\rm dc}^2\Gamma_1\alpha_{12}\big)\theta_1 - V_{\rm dc}^2\Gamma_1\alpha_{13}u_1\\ &\quad= -\mu_1 D_0\theta_0 - 2m_{11}D_0D_1\theta_0\\ &\qquad+ V_{\rm dc}^2\Gamma_1\big(\alpha_{15}\theta_0^2 + \alpha_{14}\theta_0u_0 + \alpha_{16}u_0^2\big)\\ &\qquad+ V_{\rm ac}V_{\rm dc}\Gamma_1\alpha_{11}\big(e^{i\Omega T_0} + e^{-i\Omega T_0}\big),\\ &m_{22}D_0^2u_1 + \big(k_{22} - V_{\rm dc}^2\Gamma_2\alpha_{23}\big)u_1 - V_{\rm dc}^2\Gamma_2\alpha_{22}\theta_1\\ &\quad= -\mu_2 D_0u_0 - 2m_{22}D_0D_1u_0\\ &\qquad+ V_{\rm dc}^2\Gamma_2\big(\alpha_{25}\theta_0^2 + \alpha_{24}\theta_0u_0 + \alpha_{26}u_0^2\big)\\ &\qquad+ V_{\rm ac}V_{\rm dc}\Gamma_2\alpha_{21}\big(e^{i\Omega T_0} + e^{-i\Omega T_0}\big);\end{aligned} \tag{17b}$$

$O(\varepsilon^3)$:

$$
\begin{aligned}
&m_{11}D_0^2\theta_2 + \big(k_{11} - V_{\mathrm{dc}}^2\Gamma_1\alpha_{12}\big)\theta_2 - V_{\mathrm{dc}}^2\Gamma_1\alpha_{13}u_2 \\
&\quad = -\mu_1(D_0\theta_1 + D_1\theta_0) \\
&\qquad - m_{11}\big(2D_0D_1\theta_1 + D_1^2\theta_0 + 2D_0D_2\theta_0\big) \\
&\qquad + V_{\mathrm{dc}}V_{\mathrm{ac}}\Gamma_1(\alpha_{12}\theta_0 + \alpha_{13}u_0)\big(e^{i\Omega T_0} + e^{-i\Omega T_0}\big) \\
&\qquad + V_{\mathrm{dc}}^2\Gamma_1\big(\alpha_{19}\theta_0^3 + 2\alpha_{15}\theta_0\theta_1 + \alpha_{18}\theta_0^2u_0 \\
&\qquad + \alpha_{14}\theta_1u_0 + \alpha_{17}\theta_0u_0^2 + \alpha_{110}u_0^3 \\
&\qquad + \alpha_{14}\theta_0u_1 + 2\alpha_{16}u_0u_1\big), \qquad (17c) \\
&m_{22}D_0^2u_2 + \big(k_{22} - V_{\mathrm{dc}}^2\Gamma_2\alpha_{23}\big)u_2 - V_{\mathrm{dc}}^2\Gamma_2\alpha_{22}\theta_2 \\
&\quad = -\mu_2(D_0u_1 + D_1u_0) \\
&\qquad - m_{22}\big(2D_0D_1u_1 + D_1^2u_0 + 2D_0D_2u_0\big) \\
&\qquad + V_{\mathrm{dc}}V_{\mathrm{ac}}\Gamma_2(\alpha_{22}\theta_0 + \alpha_{23}u_0)\big(e^{i\Omega T_0} + e^{-i\Omega T_0}\big) \\
&\qquad + V_{\mathrm{dc}}^2\Gamma_2\big(\alpha_{29}\theta_0^3 + 2\alpha_{25}\theta_0\theta_1 + \alpha_{28}\theta_0^2u_0 \\
&\qquad + \alpha_{24}\theta_1u_0 + \alpha_{27}\theta_0u_0^2 + \alpha_{210}u_0^3 + \alpha_{24}\theta_0u_1 \\
&\qquad + 2\alpha_{26}u_0u_1\big).
\end{aligned}
$$

Equations (17a) constitute a system of two linearly coupled differential equations with constant coefficients. Their solution can be written as

$$
\begin{bmatrix}\theta_0\\ u_0\end{bmatrix} = \begin{bmatrix}1\\ k_1\end{bmatrix} A_1(T_1,T_2)e^{i\omega_1T_0} + \begin{bmatrix}1\\ k_2\end{bmatrix} A_2(T_1,T_2)e^{i\omega_2T_0} + \mathrm{cc} \qquad (18)
$$

where cc stands for the complex conjugate of the preceding terms. The eigenfrequencies ω_1 and ω_2 are obtained from the solution of the following characteristic equation:

$$
\mathcal{D}(\omega) = \omega^4 + B\omega^2 + C = 0 \qquad (19)
$$

where

$$
\begin{aligned}
B &= \frac{1}{m_{11}m_{22}}\big[V_{\mathrm{dc}}^2(\Gamma_1\alpha_{12}m_{22} + \Gamma_2\alpha_{23}m_{11}) \\
&\quad - k_{11}m_{22} - k_{22}m_{11}\big], \\
C &= \frac{1}{m_{11}m_{22}}\big[V_{\mathrm{dc}}^4\Gamma_1\Gamma_2(\alpha_{23}\alpha_{12} - \alpha_{13}\alpha_{22}) \\
&\quad - V_{\mathrm{dc}}^2(k_{11}\Gamma_2\alpha_{23} + k_{22}\Gamma_1\alpha_{12}) + k_{11}k_{22}\big],
\end{aligned}
$$

and

$$
k_n = \frac{\alpha_{22}\Gamma_2V_{\mathrm{dc}}^2}{k_{22} - V_{\mathrm{dc}}^2\alpha_{23}\Gamma_2 - m_{22}\omega_n^2}, \quad n = 1, 2.
$$

Figure 3 displays variation of the two natural frequencies of the micromirror with the applied DC voltage V_{dc} and obtained via (19). As the DC voltage

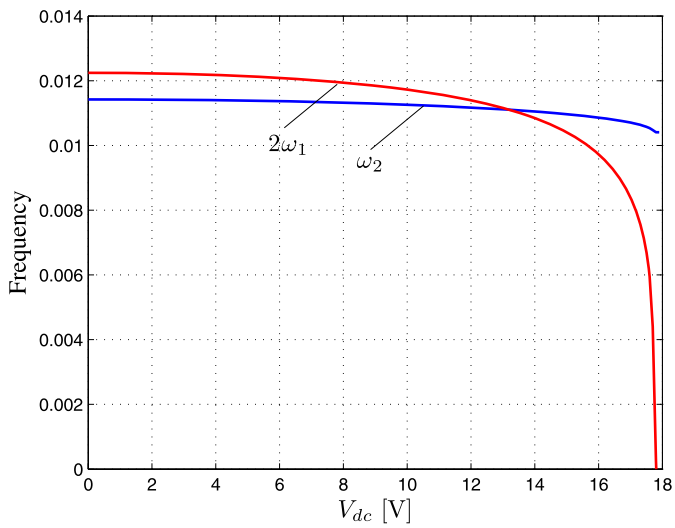

Fig. 3 Variation of the micromirror first two (dimensionless) natural frequencies with V_{dc}

is increased, the frequencies associated with the two modes decrease. The frequency of the first mode, which is purely a torsional mode at zero DC voltage, drops faster than that of the second mode (a purely bending mode at zero DC voltage) reaching zero at pull-in.[1] For the given micromirror dimensions and electrode parameters, variation of the frequencies with the applied voltage causes the frequency of the second mode to match twice the frequency of the first mode (i.e., $\omega_2 = 2\omega_1$) at $V_{\rm dc} \approx 13.2$ V. Hence, a two-to-one internal resonance might be activated between the two modes. It is important to note that this point varies with the micromirror design parameters.

3.1 Primary resonance of the first mode $\Omega \approx \omega_1$

To express the nearness of the excitation frequency Ω to the first resonant frequency ω_1, and the second resonant frequency ω_2 to twice ω_1, we write

$$\Omega = \omega_1 + \varepsilon\sigma_1, \qquad \omega_2 = 2\omega_1 + \varepsilon\sigma_2 \tag{20}$$

where σ_1 and σ_2 are frequency detuning parameters and ω_1 and ω_2 are the natural frequencies associated with the first two vibration modes corresponding to $V_{\rm dc}$. Substituting (18) and (20) into (17b) yields

$$\begin{aligned}
&m_{11}D_0^2\theta_1 + \big(k_{11} - V_{\rm dc}^2\Gamma_1\alpha_{12}\big)\theta_1 - V_{\rm dc}^2\Gamma_1\alpha_{13}u_1 \\
&\quad = -i\mu_1\big(A_1\omega_1 e^{i\omega_1 T_0} + A_2\omega_2 e^{i\omega_2 T_0}\big) \\
&\qquad - 2im_{11}\big(\omega_1 e^{i\omega_1 T_0}D_1A_1 + \omega_2 e^{i\omega_2 T_0}D_1A_2\big) \\
&\qquad + b_{11}A_1^2 e^{2i\omega_1 T_0} + b_{12}A_2^2 e^{2i\omega_2 T_0} \\
&\qquad + b_{13}A_1A_2 e^{i(\omega_1+\omega_2)T_0} + b_{13}A_1\bar{A}_2 e^{i(\omega_1-\omega_2)T_0} \\
&\qquad + b_{11}A_1\bar{A}_1 + b_{12}A_2\bar{A}_2 + \Gamma_1\alpha_{11}V_{\rm dc}V_{\rm ac}e^{i\Omega T_0} \\
&\qquad + {\rm cc},
\end{aligned} \tag{21a}$$

$$\begin{aligned}
&m_{22}D_0^2u_1 + \big(k_{22} - V_{\rm dc}^2\Gamma_2\alpha_{23}\big)u_1 - V_{\rm dc}^2\Gamma_2\alpha_{22}\theta_1 \\
&\quad = -i\mu_2\big(k_1A_1\omega_1 e^{i\omega_1 T_0} + k_2A_2\omega_2 e^{i\omega_2 T_0}\big) \\
&\qquad - 2im_{22}\big(k_1\omega_1 e^{i\omega_1 T_0}D_1A_1 + \omega_2k_2 e^{i\omega_2 T_0}D_1A_2\big) \\
&\qquad + b_{21}A_1^2 e^{2i\omega_1 T_0} + b_{22}A_2^2 e^{2i\omega_2 T_0} \\
&\qquad + b_{23}A_1A_2 e^{i(\omega_1+\omega_2)T_0} + b_{23}A_1\bar{A}_2 e^{i(\omega_1-\omega_2)T_0} \\
&\qquad + b_{21}A_1\bar{A}_1 + b_{22}A_2\bar{A}_2 + \Gamma_2\alpha_{21}V_{\rm dc}V_{\rm ac}e^{i\Omega T_0} \\
&\qquad + {\rm cc},
\end{aligned} \tag{21b}$$

[1] A detailed modal analysis of the mirror and the associated mode shapes for different DC voltages can be found in [26].

where $\bar{A}_n(T_1, T_2)$ is the complex conjugate of $A_n(T_1, T_2)$ and the coefficients b_{ij} are given by

$$\begin{aligned}
b_{n1} &= V_{\rm dc}^2\Gamma_n\big(k_1\alpha_{n4} + \alpha_{n5} + k_1^2\alpha_{n6}\big), \\
b_{n2} &= V_{\rm dc}^2\Gamma_n\big(k_2\alpha_{n4} + \alpha_{n5} + k_2^2\alpha_{n6}\big), \\
b_{n3} &= V_{\rm dc}^2\Gamma_n\big[(k_1+k_2)\alpha_{n4} + 2\alpha_{n5} + 2k_1k_2\alpha_{n6}\big], \\
&\quad n = 1, 2.
\end{aligned} \tag{22}$$

The terms proportional to $e^{\pm i\omega_1 T_0}$ and $e^{\pm i\omega_2 T_0}$ produce secular terms in θ_1 and u_1. Elimination of these terms on the right-hand side of (21a) and (21b) yields the following solvability conditions:

$$\begin{aligned}
2i\omega_1\Lambda_{11}D_1A_1 &= i\omega_1\Lambda_{12}A_1 + V_{\rm ac}\Lambda_{13}e^{i\sigma_1 T_1} \\
&\quad + \Lambda_{14}\bar{A}_1A_2e^{i\sigma_2 T_1}, \\
2i\omega_2\Lambda_{21}D_1A_2 &= i\omega_2\Lambda_{22}A_2 + \Lambda_{24}A_1^2e^{-i\sigma_2 T_1},
\end{aligned} \tag{23}$$

where

$$\begin{aligned}
\Lambda_{n1} &= k_nm_{22}\Delta_1(\omega_n) - \alpha_{22}\Gamma_2m_{11}V_{\rm dc}^2, \\
\Lambda_{n2} &= k_n\mu_2\Delta_1(\omega_n) - \alpha_{22}\Gamma_2\mu_1V_{\rm dc}^2, \\
\Lambda_{n3} &= V_{\rm dc}\big[\Gamma_2\alpha_{21}\Delta_1(\omega_n) - \alpha_{22}\alpha_{11}\Gamma_1\Gamma_2V_{\rm dc}^2\big], \\
\Lambda_{14} &= 2\Lambda_{24} = b_{11}V_{\rm dc}^2\Gamma_2\alpha_{22} + b_{21}\Delta_1(\omega_1)
\end{aligned} \tag{24}$$

and

$$\begin{aligned}
\Delta_1(\omega) &= k_{11} - \alpha_{12}V_{\rm dc}^2 - m_{11}\omega^2, \\
\Delta_2(\omega) &= k_{22} - \alpha_{23}V_{\rm dc}^2 - m_{22}\omega^2.
\end{aligned} \tag{25}$$

We substitute for D_1A_1 and D_1A_2 back into (21a) and (21b) and write the complete solution of the second-order equations as

$$\begin{aligned}
\theta_1 &= B_1(T_1, T_2)e^{i\omega_1 T_0} + B_2(T_1, T_2)e^{i\omega_2 T_0} \\
&\quad + c_{11}A_2^2e^{2i\omega_2 T_0} + c_{12}A_1A_2e^{i(\omega_1+\omega_2)T_0} \\
&\quad + c_{131}A_1\bar{A}_1 + c_{132}A_2\bar{A}_2 + {\rm cc}, \\
u_1 &= k_1B_1(T_1, T_2)e^{i\omega_1 T_0} + k_2B_2(T_1, T_2)e^{i\omega_2 T_0} \\
&\quad + c_{21}A_2^2e^{2i\omega_2 T_0} + c_{22}A_1A_2e^{i(\omega_1+\omega_2)T_0} \\
&\quad + c_{231}A_1\bar{A}_1 + c_{232}A_2\bar{A}_2 + {\rm cc}.
\end{aligned} \tag{26}$$

The first two terms in each of (26) correspond to the homogeneous solution, whereas the remaining terms represent the particular solutions. The temporal functions B_1 and B_2 are defined at the next level, and the coefficients c_{ij} are given by

$$
\begin{aligned}
c_{11} &= \frac{b_{12}[\mathcal{D}(2\omega_1)+\Delta_1(2\omega_1)\Delta_2(2\omega_1)]+b_{11}\Delta_2(2\omega_1)\Gamma_2\alpha_{22}V_{\mathrm{dc}}^2}{V_{\mathrm{dc}}^2\alpha_{22}\Gamma_2\mathcal{D}(2\omega_1)}, \qquad c_{21} = \frac{b_{11}\Gamma_2\alpha_{22}V_{\mathrm{dc}}^2+b_{12}\Delta_1(2\omega_1)}{\mathcal{D}(2\omega_1)},\\
c_{12} &= \frac{b_{23}\mathcal{D}(\omega_1+\omega_2)+\Delta_2(\omega_1+\omega_2)(\Gamma_2\alpha_{22}b_{13}V_{\mathrm{dc}}^2+b_{23}\Delta_1(\omega_1+\omega_2)^2)}{V_{\mathrm{dc}}^2\alpha_{22}\Gamma_2\mathcal{D}(\omega_1+\omega_2)},\\
c_{22} &= \frac{\Gamma_2\alpha_{22}b_{13}V_{\mathrm{dc}}^2+b_{23}\Delta_1(\omega_1+\omega_2)^2}{\mathcal{D}(\omega_1+\omega_2)},\\
c_{13n} &= \frac{b_{1n}\Delta_2(0)+\alpha_{13}\Gamma_1V_{\mathrm{dc}}^2b_{2n}}{\mathcal{D}(0)}, \qquad c_{23n} = -\frac{b_{1n}\Delta_1(0)-\alpha_{22}\Gamma_2V_{\mathrm{dc}}^2b_{2n}}{\mathcal{D}(0)}, \quad n=1,2.
\end{aligned}
\tag{27}
$$

Substituting (18) and (26) into (17c), and eliminating the terms that lead to secular terms, we obtain

$$
\begin{aligned}
&-2i\omega_1\Lambda_{11}(D_1B_1+D_2A_1)-\Lambda_{11}D_1^2A_1-\Lambda_{12}D_1A_1\\
&\quad=i\omega_1\Lambda_{12}B_1+\hat{\Lambda}_{13}V_{\mathrm{ac}}A_2e^{i(\sigma_2-\sigma_1)T_1}\\
&\qquad+\Lambda_{14}(A_2\bar{B}_1+B_2\bar{A}_1)e^{i\sigma_2T_1}\\
&\qquad+\hat{\Lambda}_{15}\bar{A}_1A_1^2+\hat{\Lambda}_{16}A_1A_2\bar{A}_2,\\
&-2i\omega_2\Lambda_{21}(D_1B_2+D_2A_2)-\Lambda_{21}D_1^2A_2-\Lambda_{22}D_1A_2\\
&\quad=i\omega_2\Lambda_{22}B_2+\hat{\Lambda}_{23}V_{\mathrm{ac}}A_1e^{i(\sigma_1-\sigma_2)T_1}\\
&\qquad+\hat{\Lambda}_{25}\bar{A}_2A_2^2+\hat{\Lambda}_{26}A_1\bar{A}_1A_2,
\end{aligned}
\tag{28}
$$

where

$$
\begin{aligned}
\hat{\Lambda}_{13} &= V_{\mathrm{dc}}\Gamma_2\big[\alpha_{22}\Delta_2(\omega_1)-k_2\Gamma_2\alpha_{23}\Delta_1(\omega_1)\big],\\
\hat{\Lambda}_{23} &= V_{\mathrm{dc}}\Gamma_2\big[\alpha_{22}\Delta_2(\omega_2)-k_1\Gamma_2\alpha_{23}\Delta_1(\omega_1)\big],\\
\hat{\Lambda}_{15} &= -V_{\mathrm{dc}}^2\big(\Delta_1(\omega_1)Z_2-\Gamma_2\alpha_{22}V_{\mathrm{dc}}^2Z_1\big),\\
\hat{\Lambda}_{25} &= -V_{\mathrm{dc}}^2\big(\Delta_1(\omega_1)\tilde{Z}_2-\Gamma_2\alpha_{22}V_{\mathrm{dc}}^2\tilde{Z}_1\big),\\
\hat{\Lambda}_{16} &= -V_{\mathrm{dc}}^2\big(\Delta_1(\omega_1)Y_2-\Gamma_2\alpha_{22}V_{\mathrm{dc}}^2Y_1\big),\\
\hat{\Lambda}_{26} &= -V_{\mathrm{dc}}^2\big(\Delta_1(\omega_1)\tilde{Y}_2-\Gamma_2\alpha_{22}V_{\mathrm{dc}}^2\tilde{Y}_1\big),
\end{aligned}
$$

and Z_n, $\tilde{Z}_n$, Y_n, and $\tilde{Y}_n$ are given by

$$
\begin{aligned}
Z_n &= \Gamma_n\big[2c_{131}(\alpha_{n4}+2\alpha_{n5})+2c_{231}(\alpha_{n4}+2k_1\alpha_{n6})\\
&\qquad+3\big(k_1^3\alpha_{n10}+k_1^2\alpha_{n7}+k_1\alpha_{n8}+\alpha_{n9}\big)\big],\\
\tilde{Z}_n &= \Gamma_n\big[2c_{132}(\alpha_{n4}+2\alpha_{n5})+2c_{232}(\alpha_{n4}+2k_2\alpha_{n6})\\
&\qquad+3\big(k_2^3\alpha_{n10}+k_2^2\alpha_{n7}+k_2\alpha_{n8}+\alpha_{n9}\big)\big],
\end{aligned}
$$

$$
\begin{aligned}
Y_n &= \Gamma_n\big[\alpha_{n4}(c_{22}+2c_{132}+2c_{131}k_1+k_2c_{12})\\
&\qquad+\alpha_{n5}(2c_{21}+4c_{132})+\alpha_{n6}(2c_{22}k_2+4c_{232}k_1)\\
&\qquad+\alpha_{n7}(2k_2^2+4k_2k_1)+\alpha_{n8}(4k_2+2k_1)\\
&\qquad+6\alpha_{n9}+\alpha_{n10}\big(6k_2^2k_1\big)\big],\\
\tilde{Y}_n &= \Gamma_n\big[\alpha_{n4}(c_{22}+2c_{231}+2c_{131}k_2+k_1c_{12})\\
&\qquad+\alpha_{n5}(2c_{12}+4c_{131})+\alpha_{n6}(2c_{22}k_1+4c_{231}k_2)\\
&\qquad+\alpha_{n7}(2k_1^2+4k_1k_2)+\alpha_{n8}(4k_1+2k_2)\\
&\qquad+6\alpha_{n9}+\alpha_{n10}\big(6k_1^2k_2\big)\big], \quad n=1,2.
\end{aligned}
\tag{29}
$$

Following Nayfeh [27], we choose the functions B_1 and B_2 so as to eliminate $D_1^2A_1$ and $D_1^2A_2$ from (28), thereby ensuring that, in the absence of damping, (28) are derivable from a Lagrangian. These conditions lead to

$$
\begin{aligned}
D_1[2i\omega_1B_1+D_1A_1] &= 0,\\
D_1[2i\omega_2B_2+D_1A_2] &= 0,
\end{aligned}
\tag{30}
$$

which, upon integration with respect to T_1, yields

$$
\begin{aligned}
[2i\omega_1B_1+D_1A_1] &= c_1(T_2),\\
[2i\omega_2B_2+D_1A_2] &= c_2(T_2).
\end{aligned}
\tag{31}
$$

We note from (23) that D_1A_1 and D_1A_2 are not explicit functions of T_2. Therefore, it is necessary that $c_1(T_2)=c_2(T_2)=0$, which yields

$$
\begin{aligned}
B_1 &= i\frac{\Lambda_{12}}{4\omega_1\Lambda_{11}}A_1+V_{\mathrm{ac}}\frac{\Lambda_{13}}{4\omega_1^2\Lambda_{11}}e^{i\sigma_1T_1}\\
&\qquad+\frac{\Lambda_{14}}{4\omega_1^2\Lambda_{11}}\bar{A}_1A_2e^{i\sigma_2T_1},
\end{aligned}
\tag{32}
$$

$$B_2 = i\frac{\Lambda_{22}}{4\omega_2\Lambda_{21}}A_2 + \frac{\Lambda_{24}}{4\omega_2^2\Lambda_{21}}A_1^2 e^{-i\sigma_2 T_1}.$$

Substituting (33) into (28), we obtain

$$\begin{aligned}
&-2i\omega_1\Lambda_{11}D_2A_1 \\
&\quad = \frac{\Lambda_{12}^2}{4\Lambda_{11}}A_1 - iV_{\mathrm{ac}}\frac{\Lambda_{12}\Lambda_{13}}{4\omega_1\Lambda_{11}}e^{i\sigma_1 T_1} \\
&\qquad + V_{\mathrm{ac}}\left(\hat{\Lambda}_{13} + \frac{\Lambda_{13}\Lambda_{14}}{4\omega_1^2\Lambda_{11}}\right)A_2 e^{i(\sigma_2-\sigma_1)T_1} \\
&\qquad + i\frac{\Lambda_{22}\Lambda_{14}}{2\omega_2\Lambda_{21}}A_2\bar{A}_1 e^{i\sigma_2 T_1} \\
&\qquad + \left(\hat{\Lambda}_{15} + \frac{\Lambda_{24}\Lambda_{14}}{4\omega_2^2\Lambda_{21}}\right)\bar{A}_1 A_1^2 \\
&\qquad + \left(\hat{\Lambda}_{16} + \frac{\Lambda_{14}^2}{4\omega_1^2\Lambda_{11}}\right)A_1 A_2\bar{A}_2, \qquad (33a)
\end{aligned}$$

$$\begin{aligned}
&-2i\omega_2\Lambda_{21}D_2A_2 \\
&\quad = \frac{\Lambda_{22}^2}{4\Lambda_{21}}A_2 - i\frac{\Lambda_{22}\Lambda_{24}}{4\omega_2\Lambda_{21}}A_1^2 e^{-i\sigma_2 T_1} \\
&\qquad + \hat{\Lambda}_{23}V_{\mathrm{ac}}A_1 e^{i(\sigma_1-\sigma_2)T_1} \\
&\qquad + \hat{\Lambda}_{25}\bar{A}_2 A_2^2 + \hat{\Lambda}_{26}A_1\bar{A}_1 A_2. \qquad (33b)
\end{aligned}$$

Since the above equations should be derivable from a Lagrangian and a virtual work term [28], the coefficient associated with $A_2\bar{A}_1$ in (33a) should be twice the coefficient associated with A_1^2 in (33b). Similarly, the coefficient associated with $A_1A_2\bar{A}_2$ in (33a) should be equal to the coefficient associated with $A_2A_1\bar{A}_1$ in (33b).

To obtain the final solution to second order, we reconstitute the solution using the following equation:

$$\frac{dA_n}{dt} = \varepsilon D_1 A_n + \varepsilon^2 D_2 A_n + \cdots, \quad n = 1, 2. \qquad (34)$$

We substitute (23), (33a), (33b) into (34), set $T_n = \varepsilon^n t$, then set ε equal to unity, and obtain the following reconstituted modulation equations:

$$\begin{aligned}
&-2i\omega_1\Lambda_{11}\frac{dA_1}{dt} \\
&\quad = (\mathcal{S}_{12} + i\tilde{\mathcal{S}}_{12})A_1 + (\mathcal{S}_{13} + i\tilde{\mathcal{S}}_{13})V_{\mathrm{ac}}e^{i\sigma_1 t} \\
&\qquad + \mathcal{S}_{14}V_{\mathrm{ac}}A_2 e^{i(\sigma_2-\sigma_1)t} + (\mathcal{S}_{15} + i\tilde{\mathcal{S}}_{15})A_2\bar{A}_1 e^{i\sigma_2 t} \\
&\qquad + \mathcal{S}_{16}\bar{A}_1 A_1^2 + \mathcal{S}_{17}A_1A_2\bar{A}_2, \qquad (35a)
\end{aligned}$$

$$\begin{aligned}
&-2i\omega_2\Lambda_{21}\frac{dA_2}{dt} \\
&\quad = (\mathcal{S}_{22} + i\tilde{\mathcal{S}}_{22})A_2 + (\mathcal{S}_{25} - i\tilde{\mathcal{S}}_{25})A_1^2 e^{-i\sigma_2 t} \\
&\qquad + \mathcal{S}_{24}V_{\mathrm{ac}}A_1 e^{i(\sigma_1-\sigma_2)t} + \mathcal{S}_{26}\bar{A}_2 A_2^2 \\
&\qquad + \mathcal{S}_{27}A_1\bar{A}_1 A_2, \qquad (35b)
\end{aligned}$$

where

$$\mathcal{S}_{n2} = \frac{\Lambda_{n2}^2}{4\Lambda_{n1}}, \qquad \tilde{\mathcal{S}}_{n2} = -\Lambda_{n2}\omega_n,$$

$$\mathcal{S}_{13} = -\Lambda_{13}, \qquad \tilde{\mathcal{S}}_{13} = -\frac{\Lambda_{12}\Lambda_{13}}{4\omega_1\Lambda_{11}},$$

$$\mathcal{S}_{14} = \left(\hat{\Lambda}_{13} + \frac{\Lambda_{13}\Lambda_{14}}{4\omega_1^2\Lambda_{11}}\right), \qquad \mathcal{S}_{24} = \hat{\Lambda}_{23},$$

$$\mathcal{S}_{15} = 2\mathcal{S}_{25} = -2\Lambda_{24}, \qquad \tilde{\mathcal{S}}_{15} = 2\tilde{\mathcal{S}}_{25} = \frac{\Lambda_{22}\Lambda_{14}}{2\omega_2\Lambda_{21}},$$

$$\mathcal{S}_{16} = \left(\hat{\Lambda}_{15} + \frac{\Lambda_{24}\Lambda_{14}}{4\omega_2^2\Lambda_{21}}\right), \qquad \mathcal{S}_{26} = \hat{\Lambda}_{25},$$

$$\mathcal{S}_{17} = \mathcal{S}_{27} = \left(\hat{\Lambda}_{16} + \frac{\Lambda_{14}^2}{4\omega_1^2\Lambda_{11}}\right), \qquad n = 1, 2.$$

We find it convenient to express the resulting modulation equations in polar form by introducing the following transformation:

$$A_n = \frac{1}{2}a_n e^{i\beta_n} \quad n = 1, 2, \qquad (36)$$

where the a_n and β_n are real functions of time. Inserting (36) into (35a) and (35b) and separating the real and imaginary parts, we obtain

$$\begin{aligned}
\omega_1\Lambda_{11}\dot{a}_1 &= -\frac{1}{2}\tilde{\mathcal{S}}_{12}a_1 - V_{\mathrm{ac}}(\mathcal{S}_{13}\sin\gamma_1 + \tilde{\mathcal{S}}_{13}\cos\gamma_1) \\
&\quad + \frac{1}{2}\mathcal{S}_{14}V_{\mathrm{ac}}a_2\sin(\gamma_1-\gamma_2) \\
&\quad - \frac{1}{4}a_1a_2(\mathcal{S}_{15}\sin\gamma_2 + \tilde{\mathcal{S}}_{15}\cos\gamma_2), \\
\omega_1\Lambda_{11}a_1(\sigma_1 - \dot{\gamma}_1) &= \frac{1}{2}\mathcal{S}_{12}a_1 + V_{\mathrm{ac}}(\mathcal{S}_{13}\cos\gamma_1 + \tilde{\mathcal{S}}_{13}\sin\gamma_1) \\
&\quad - \frac{1}{2}V_{\mathrm{ac}}\mathcal{S}_{14}a_2\cos(\gamma_1-\gamma_2) \\
&\quad + \frac{1}{4}a_1a_2(\mathcal{S}_{15}\cos\gamma_2 - \tilde{\mathcal{S}}_{15}\sin\gamma_2) \\
&\quad + \frac{1}{8}\mathcal{S}_{16}a_1^3 + \frac{1}{8}\mathcal{S}_{17}a_1a_2^2,
\end{aligned} \qquad (37a)$$

$$\omega_2 \Lambda_{21} \dot{a}_2 = -\frac{1}{2}\tilde{\mathcal{S}}_{22} a_2 - \frac{1}{2}\mathcal{S}_{24} V_{\mathrm{ac}} a_1 \sin(\gamma_1 - \gamma_2) + \frac{1}{4} a_1^2 (\mathcal{S}_{25} \sin\gamma_2 - \tilde{\mathcal{S}}_{25} \cos\gamma_2),$$

$$\omega_2 \Lambda_{21} a_2 (\dot{\gamma}_2 - \dot{\gamma}_1 + 2\sigma_1 - \sigma_2) = \frac{1}{2}\mathcal{S}_{22} a_2 + \frac{1}{2} V_{\mathrm{ac}} \mathcal{S}_{24} a_1 \cos(\gamma_1 - \gamma_2) + \frac{1}{4} a_1^2 (\mathcal{S}_{25} \cos\gamma_2 + \tilde{\mathcal{S}}_{25} \sin\gamma_2) + \frac{1}{8}\mathcal{S}_{26} a_2^3 + \frac{1}{8}\mathcal{S}_{27} a_1^2 a_2, \tag{37b}$$

where

$$\gamma_1 = \sigma_1 t - \beta_1, \qquad \gamma_2 = \sigma_2 t - 2\beta_1 + \beta_2.$$

Using (36), we express the response of the mirror to second order as

$$\begin{aligned}\theta(t) = \theta_s &+ \left(1 + \frac{\mathcal{S}_{11}}{\omega_1}\right) a_1 \cos(\omega_1 t + \beta_1) \\ &+ \left(1 + \frac{\mathcal{S}_{21}}{\omega_2}\right) a_2 \cos(\omega_2 t + \beta_2) \\ &+ \frac{\Lambda_{14}}{8\omega_1^2 \Lambda_{11}} a_1 a_2 \cos\big[(\omega_1 + \sigma_2)t + \beta_2 - \beta_1\big] \\ &+ \frac{1}{2} c_{12} a_1 a_2 \cos\big[(\omega_1 + \omega_2)t + \beta_1 + \beta_2\big] \\ &+ \frac{\Lambda_{24}}{8\omega_2^2 \Lambda_{21}} a_1^2 \cos\big[(\omega_2 - \sigma_2)t + 2\beta_1\big] \\ &+ \frac{1}{2} c_{11} a_2^2 \cos[2\omega_2 t + 2\beta_2] + \frac{1}{2} c_{13} a_1^2 \\ &+ \frac{1}{2} c_{14} a_1 a_2 + V_{\mathrm{ac}} \frac{\tilde{\mathcal{S}}_{13}}{\Lambda_{12}\omega_1} \cos\big[(\omega_1 + \sigma_1)t\big] \\ &+ \cdots, \end{aligned} \tag{38a}$$

$$\begin{aligned}u(t) = u_s &+ k_1 \left(1 + \frac{\mathcal{S}_{11}}{\omega_1}\right) a_1 \cos(\omega_1 t + \beta_1) \\ &+ k_2 \left(1 + \frac{\mathcal{S}_{21}}{\omega_2}\right) a_2 \cos(\omega_2 t + \beta_2) \\ &+ k_1 \frac{\Lambda_{14}}{8\omega_1^2 \Lambda_{11}} a_1 a_2 \cos\big[(\omega_1 + \sigma_2)t + \beta_2 - \beta_1\big] \\ &+ \frac{1}{2} c_{22} a_1 a_2 \cos\big[(\omega_1 + \omega_2)t + \beta_1 + \beta_2\big] \\ &+ k_2 \frac{\Lambda_{24}}{8\omega_2^2 \Lambda_{21}} a_1^2 \cos\big[(\omega_2 - \sigma_2)t + 2\beta_1\big] \\ &+ \frac{1}{2} c_{21} a_2^2 \cos(2\omega_2 t + 2\beta_2) + \frac{1}{2} c_{23} a_1^2 \\ &+ \frac{1}{2} c_{24} a_1 a_2 \\ &+ k_1 V_{\mathrm{ac}} \frac{\tilde{\mathcal{S}}_{13}}{\Lambda_{12}\omega_1} \cos\big[(\omega_1 + \sigma_1)t\big] + \cdots. \end{aligned} \tag{38b}$$

We illustrate the effect of neglecting the interaction between the two modes on the quality of the approximation by plotting variation of the effective nonlinearity coefficient $\mathcal{S}_{16}$ with V_{dc} in Fig. 4. Using a single-mode analysis results in a singularity at $V_{\mathrm{dc}} \approx 13.2$ V, which corresponds to the location of the two-to-one internal resonance between the first and second modes. Neglecting this interaction yields a qualitatively and quantitatively erroneous solution, which might hide the actual dynamics of the mirror. The size of the neighborhood where energy is exchanged between the two modes can be inferred from the region in Fig. 4 where the one-mode approximation of $\mathcal{S}_{16}$ diverges from the two-mode approximation of $\mathcal{S}_{16}$. It can be seen in the figure that this region is not limited to a narrow band around $V_{\mathrm{dc}} \approx 13.2$ V, rather it extends over a wide range of the DC voltage. Therefore, avoiding operation in this region would place significant limits on the operation range of the microscanner.

To validate the analytical solution, we integrate (7) and (8) numerically to obtain the steady-state response of the mirror at the critical DC voltage $V_{\mathrm{dc}} = 13.21$ V when the mirror is excited near primary resonance of the first mode $\Omega = \omega_1 - 0.0002$ and $V_{\mathrm{ac}} = 0.1$ V. We then compare the numerical results with those obtained analytically using (38). The phase portraits of the steady-state response of the micromirror in Fig. 5 demonstrate excellent agreement between the numerical and analytical solutions, thereby validating the analytical solution.

The micromirror behavior is characterized by solving the modulation equations of the two-mode response. A fixed-point of the modulation equations, an equilibrium solution, corresponds to a periodic mirror response. On the other hand, when the modulation equations have a periodic solution, the response of the mirror is either periodic or quasiperiodic, depending on the frequency of the limit cycle of the modulation equations. If the frequency of this cycle is commensurate with the excitation frequency, the response is

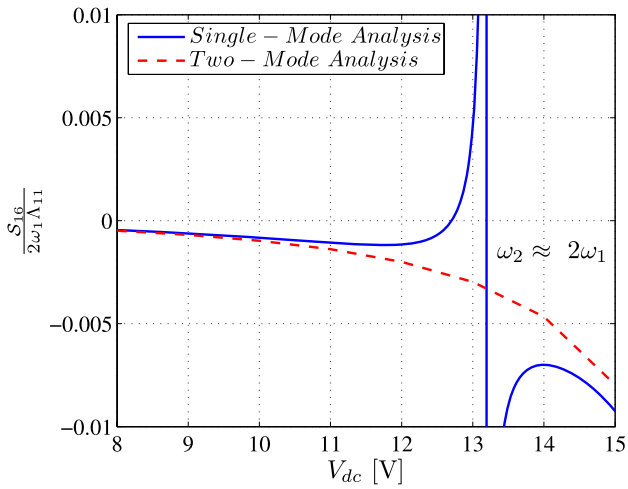

Fig. 4 Variation of the effective nonlinearity coefficient $\mathcal{S}_{16}$ with the DC voltage V_{dc}

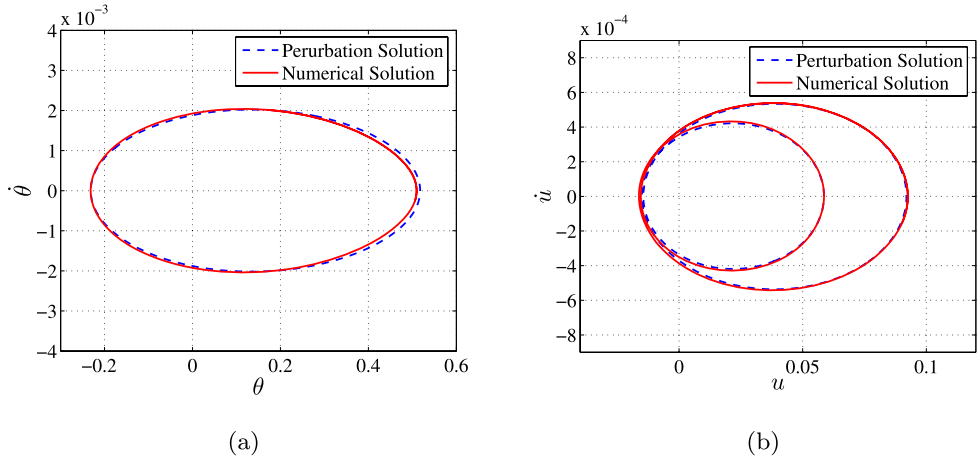

Fig. 5 Phase portrait of the micromirror response at $V_{\text{dc}} = 13.21$ V when it is excited near primary resonance of the first mode $\Omega = \omega_1 - 0.0002$ and $V_{\text{ac}} = 0.1$ V

periodic; otherwise it is quasiperiodic with two independent periods. When the modulation equations have a quasiperiodic solution, the response of the mirror is quasiperiodic with a higher number of independent periods. Finally, if the solution of the modulation equations is chaotic, then the response of the microscanner is chaotically modulated.

To determine the periodic response of the mirror, we found the equilibrium solutions of (37) by setting the time derivatives in the equations equal to zero and solving for the roots (a_1, a_2, γ_1, γ_2). As a control parameter was varied, the roots were found using a Newton–Raphson numerical technique. The stability of each equilibrium solution was determined by finding the eigenvalues of the Jacobian matrix of the modulation equations evaluated at the solution. Solutions where all of the eigenvalues have negative real parts are asymptotically stable. Solutions where one or more eigenvalues have positive real parts are unstable. We used this method to conduct a frequency sweep with respect to the detuning parameter σ_1 for different values of V_{dc} and a fixed excitation amplitude $V_{\text{ac}} = 0.1$ V. To achieve large amplitudes, microscanners are designed to operate at large quality factors, therefore we use a quality factor $Q = 250$. We denote stable equilibrium solutions by solid lines and unstable solutions by dashed or dotted lines.

At $V_{\text{dc}} = 11$ V, the response consists of a single mode except in a small range around $\sigma_1 = 0$, as shown in Fig. 6(a) and (b). Even in this range, most of the en-

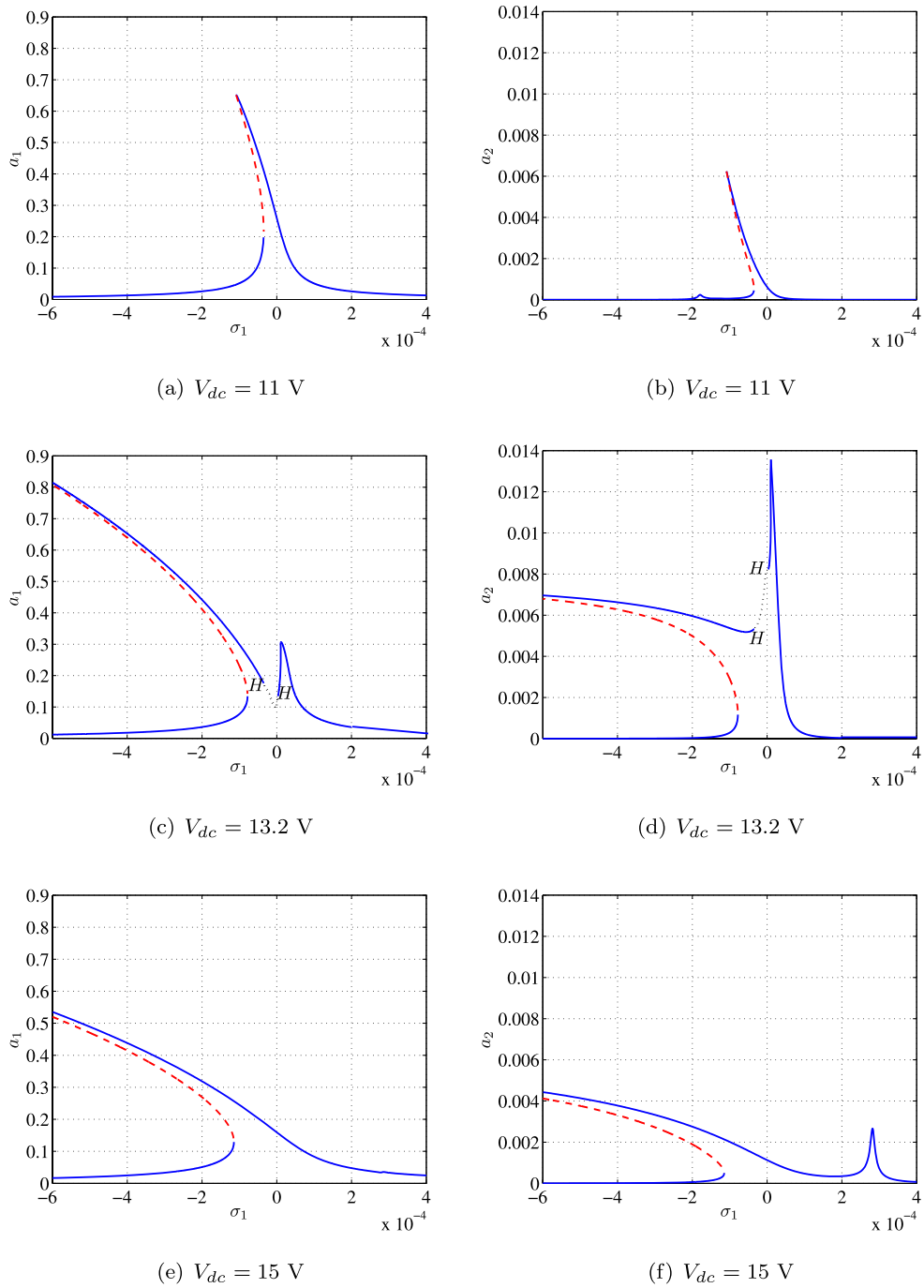

(a) $V_{dc} = 11$ V (b) $V_{dc} = 11$ V

(c) $V_{dc} = 13.2$ V (d) $V_{dc} = 13.2$ V

(e) $V_{dc} = 15$ V (f) $V_{dc} = 15$ V

Fig. 6 Frequency-response curves of the first and second modes when the first mode is excited near primary resonance at $V_{\text{ac}} = 0.1$ V. The letter H denotes a Hopf bifurcation

ergy is trapped in the first mode and the influence of the second mode is extremely small. In fact, second-mode motions are 2–3 orders of magnitude smaller than first-mode motions, as can be seen in the time histories of the response at $\sigma_1 = 0$ shown in Fig. 7(a) and (b). A small branch of solutions also appears at

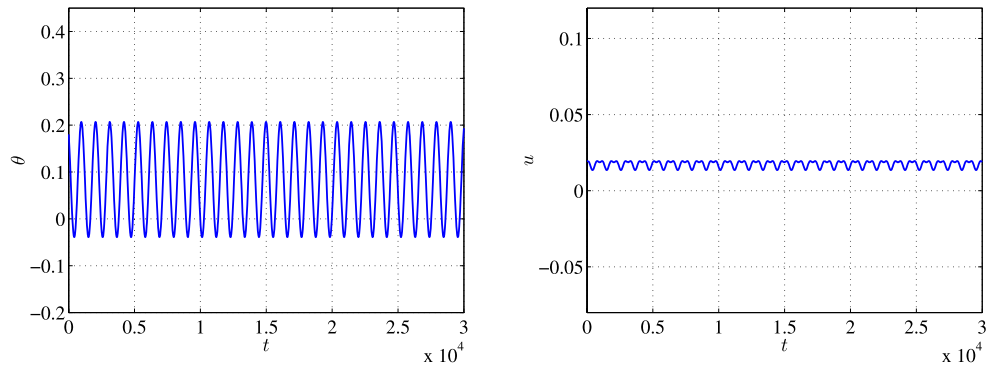

(a) $V_{dc} = 11$ V (b) $V_{dc} = 11$ V

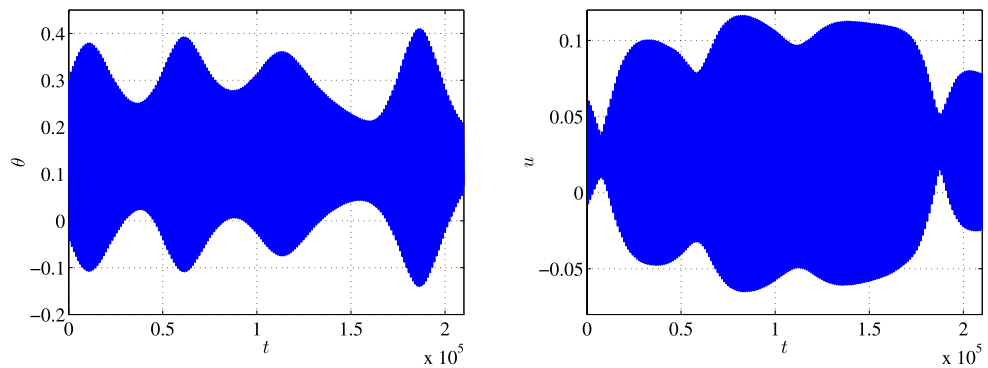

(c) $V_{dc} = 13.2$ V (d) $V_{dc} = 13.2$ V

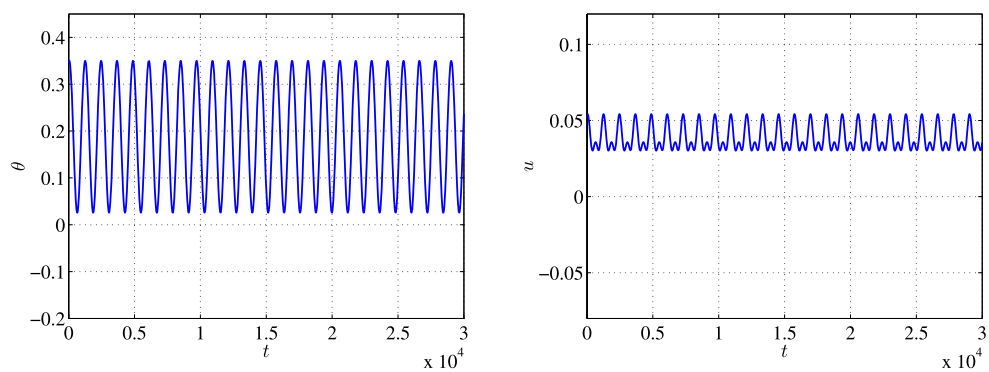

(e) $V_{dc} = 15$ V (f) $V_{dc} = 15$V

Fig. 7 Long-time histories of the micromirror responses for $\Omega = \omega_1$ and $V_{\text{ac}} = 0.1$ V

$\sigma_1 \approx -0.00018$, indicating the impending activation of internal resonance. Further, the frequency-response curves of both modes are bent to the left, indicating a softening-type nonlinearity.

As V_{dc} is increased towards the critical value $V_{\text{dc}} \approx 13.2$ V, Fig. 6(c) and (d), the frequency-response curves bend more to the left, indicating that the softening nonlinearity is increasing with V_{dc}. Further,

the second branch of the two-mode solution becomes more significant and shifts towards $\sigma_1 = 0$. A region of dynamic solutions appears as a result of the equilibrium solutions of the modulation equations losing stability via two Hopf bifurcations. This region extends between $\sigma_1 = 0$ and $\sigma_1 = -0.00002$, resulting in an undesired quasiperiodic response of the scanner, as shown in Fig. 7(c) and (d). The quasiperiodic behavior causes fluctuations in the amplitude of the steady-state response of the scanner, which brings the target surface in and out of focus while the scanned area changes over time.

A further increase in $V_{\rm dc}$, Fig. 6(e) and (f), bends the frequency-response curves further to the left and shifts the second branch of solutions further to the right and away from $\sigma_1 = 0$. As a result, the dynamic solutions disappear while the effect of the second mode becomes less important and it diminishes as $V_{\rm dc}$ increases. Figure 7(e) and (f) illustrates the periodic nature of the mirror response in this region.

3.2 Primary resonance of the second mode $\Omega \approx \omega_2$

In this case, the excitation frequency is in the neighborhood of the second natural frequency $\Omega = \omega_2 + \varepsilon\sigma_1$. We follow steps similar to those used in the previous section to obtain the following modulation equations:

$$\begin{aligned}
&\omega_1 \Lambda_{11}\dot{a}_1 = -\frac{1}{2}\tilde{\mathcal{S}}_{12}a_1 - \frac{1}{2}\mathcal{S}_{24}V_{\rm ac}a_1\sin\gamma_1 \\
&\qquad - \frac{1}{4}a_1a_2(\mathcal{S}_{15}\sin\gamma_2 + \tilde{\mathcal{S}}_{15}\cos\gamma_2), \\
&\frac{1}{2}\omega_1\Lambda_{11}a_1(\sigma_1+\sigma_2-\dot{\gamma}_1) \\
&\quad = \frac{1}{2}\mathcal{S}_{12}a_1 + \frac{1}{2}\mathcal{S}_{24}V_{\rm ac}a_1\cos\gamma_1 \\
&\qquad + \frac{1}{4}a_1a_2(\mathcal{S}_{15}\cos\gamma_2 - \tilde{\mathcal{S}}_{15}\sin\gamma_2) \\
&\qquad + \frac{1}{8}\mathcal{S}_{16}a_1^3 + \frac{1}{8}\mathcal{S}_{17}a_1a_2^2,
\end{aligned} \tag{39a}$$

$$\begin{aligned}
&\omega_2\Lambda_{21}\dot{a}_2 = -\frac{1}{2}\tilde{\mathcal{S}}_{22}a_2 - V_{\rm ac}(\mathcal{S}_{23}\sin\gamma_2 + \tilde{\mathcal{S}}_{23}\cos\gamma_2) \\
&\qquad + \frac{1}{4}a_1^2(\mathcal{S}_{25}\sin\gamma_2 - \tilde{\mathcal{S}}_{25}\cos\gamma_2), \\
&\omega_2\Lambda_{21}a_2(\sigma_1-\dot{\gamma}_2) \\
&\quad = \frac{1}{2}\mathcal{S}_{22}a_2 - V_{\rm ac}(\tilde{\mathcal{S}}_{23}\sin\gamma_2 - \mathcal{S}_{23}\cos\gamma_2) \\
&\qquad + \frac{1}{4}a_1^2(\mathcal{S}_{25}\cos\gamma_2 + \tilde{\mathcal{S}}_{25}\sin\gamma_2) \\
&\qquad + \frac{1}{8}\mathcal{S}_{26}a_2^3 + \frac{1}{8}\mathcal{S}_{27}a_1^2a_2,
\end{aligned} \tag{39b}$$

where

$$\gamma_1 = (\sigma_1+\sigma_2)t - 2\beta_1, \qquad \gamma_2 = \sigma_1 t - \beta_2.$$

In the case of primary resonance near the second mode, the equilibrium solutions of the modulation equations are either a single-mode solution $(0, a_2)$, a two-mode solution (a_1, a_2), or both. Figure 8 displays variation of the response amplitude with the driving frequency detuning parameter σ_1. For $V_{\rm dc} = 11$ V, the energy is trapped in the second mode only, as shown in Fig. 8(a) and (b). The solution of the modulation equations yields only the single-mode solution $(0, a_2)$. Therefore, the nonlinear interaction can be neglected and a single-mode solution suffices to accurately represent the dynamics of the mirror. The long-time history of the response shown in Fig. 9 illustrates that the second mode completely dominates the response of the mirror. As $V_{\rm dc}$ approaches the critical value $V_{\rm dc} = 13.2$ V, the single-mode solution loses stability, Fig. 8(c) and (d), via two pitchfork bifurcations at $\sigma_1 = -0.000073$ and $\sigma_1 = 0.000058$. A two-peak branch of two-mode solutions (a_1, a_2) appears in the frequency-response curves in the vicinity of $\sigma_1 = 0$. In this case, most of the system energy is transferred into the indirectly excited first mode and a single-mode solution is not enough to represent the dynamics of the mirror. In Fig. 10, we show the long-time histories of the response for different values of σ_1. At $\sigma_1 = 0$, there is only one two-mode solution, where a_1 is much larger than a_2. The angular response of the mirror is periodic with a period corresponding to the first-mode frequency, Fig. 10(a). However,

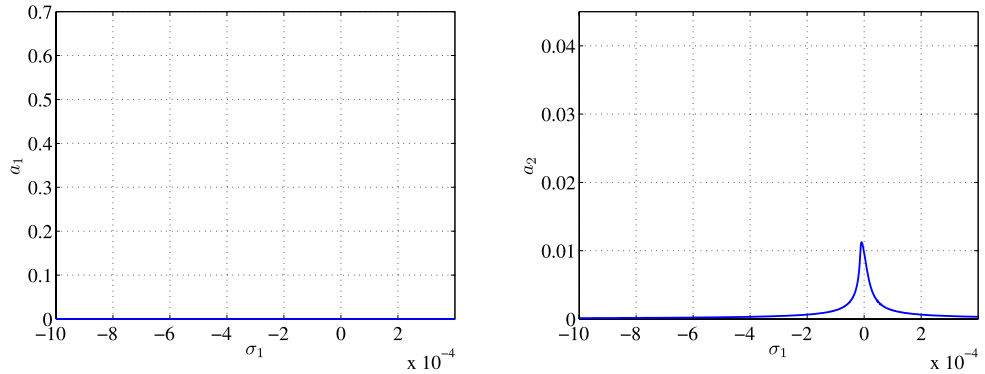

(a) $V_{dc} = 11$ V

(b) $V_{dc} = 11$ V

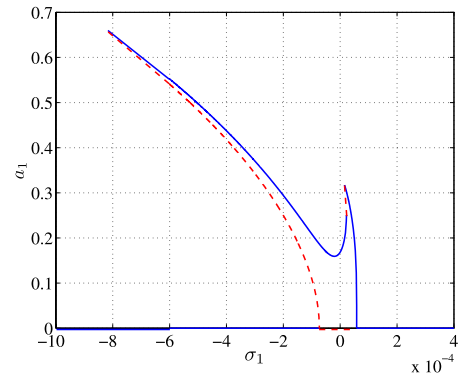

(c) $V_{dc} = 13.2$ V

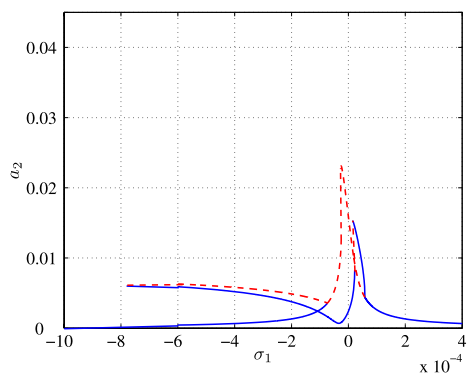

(d) $V_{dc} = 13.2$ V

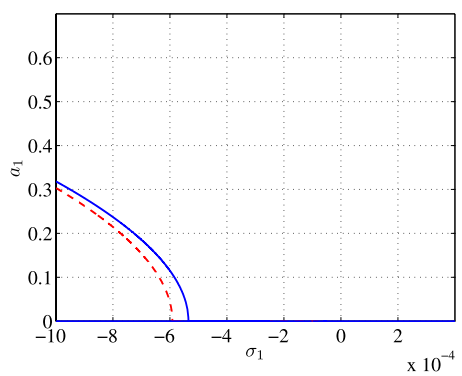

(e) $V_{dc} = 15$ V

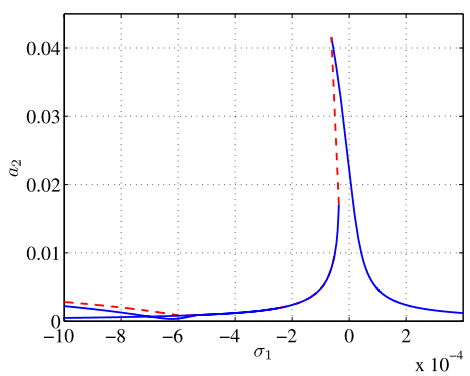

(f) $V_{dc} = 15$ V

Fig. 8 Frequency-response curves of the first and second modes when the second mode is excited near primary resonance and $V_{\text{ac}} = 0.1$ V

due to the linear coupling, the bending response of the mirror is periodic with both frequencies appearing in the response, Fig. 10(b). At $\sigma_1 = -0.0004$, both of the single-mode and two-mode solutions coexist. Therefore, the angular oscillations of the mirror can be large and dominated by the first mode, Fig. 10(c),

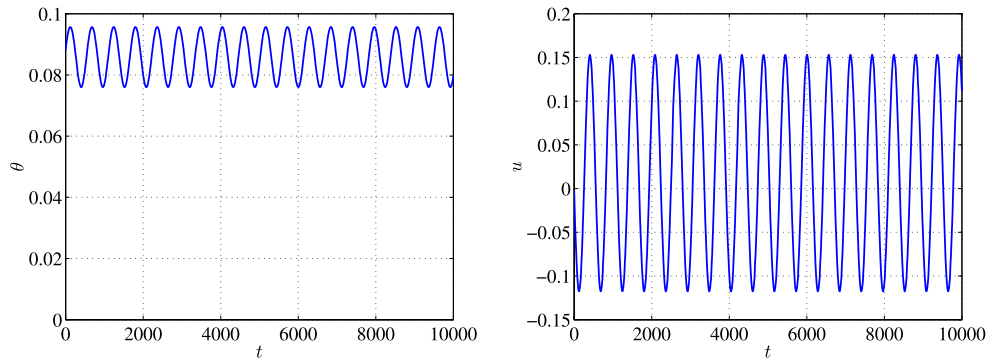

(a) $\sigma_1 = 0$ (b) $\sigma_1 = 0$

Fig. 9 Long-time histories of the micromirror response for $V_{\text{dc}} = 11$ V and $V_{\text{ac}} = 0.1$ V

or very small and dominated by the second mode, Fig. 10(e).

As V_{dc} is increased beyond the critical value, we find that the two-mode solution shifts to the left, Fig. 8(e) and (f), where the single-mode solution loses stability via two pitchfork bifurcations at $\sigma_1 \approx -0.0006$ and $\sigma_1 \approx -0.00055$. Therefore, a two-mode solution is still necessary to represent the dynamic response of the mirror. In Fig. 11(a) and (b), we show long-time histories of the micromirror response at $\sigma_1 = 0$ where the second mode dominates both of the torsional and bending responses of the mirror, resulting in a very large bending response. At $\sigma_1 = -0.0008$, both of the single-mode and two-mode solutions coexist. In Fig. 11(c) and (d), we show the long-time histories of the two-mode solution. In this case, the period of the mirror angular response corresponds to the frequency of the first-mode, whereas the frequencies of both modes appear in the bending response.

In Fig. 12(a) and (b), we show the force-response curves of the first and second modes at the critical internal resonance voltage $V_{\text{dc}} = 13.2$ V. We excite the second mode near primary resonance at the detuning value $\sigma_1 = -0.00002$. A single-mode response $(0, a_2)$ is the only available solution for $V_{\text{ac}} \leq 0.008$ V. As V_{ac} is increased, the single-mode solution loses stability through a subcritical pitchfork bifurcation at $V_{\text{ac}} \approx 0.011$ V. As a result, the response jumps to a larger stable two-mode solution. As V_{ac} is increased further, the amplitude of the first mode increases, while the amplitude of the second mode decreases slightly. However, no saturation occurs, since the quadratic and cubic nonlinearities are of the same order, and the amplitude of the second mode begins to increase again until $V_{\text{ac}} \approx 0.315$ V. At this point, the stable two-mode solution experiences a saddle-node bifurcation, and the response jumps to the nearest stable branch, which is another larger-amplitude two-mode solution. Increasing V_{ac} beyond this point results in a gradual decrease in the first-mode amplitude accompanied with a gradual increase in the second-mode amplitude.

4 Observations and comments

As demonstrated in the preceding section, this nonlinear analytical study has revealed an interesting energy transfer mechanism that is hard to identify or understand utilizing simulations, finite element methods, or even an extensive number of experiments. When activated during a scanner's operation, the internal resonance can cause serious degradation in the mirror performance. Indeed, the quasiperiodic response of the scanner which can appear when the micromirror is excited at primary resonance of the first mode, results in steady-state amplitude fluctuations that distort the scanned area and the quality of the reflected beam. On the other hand, when the mirror is excited near primary resonance of the second mode, the second-mode amplitude does not saturate due to the considerable effects of the cubic nonlinearities, resulting in large undesirable bending oscillations. Consequently, it is imperative to take this phenomenon into account during the design of future microscanners.

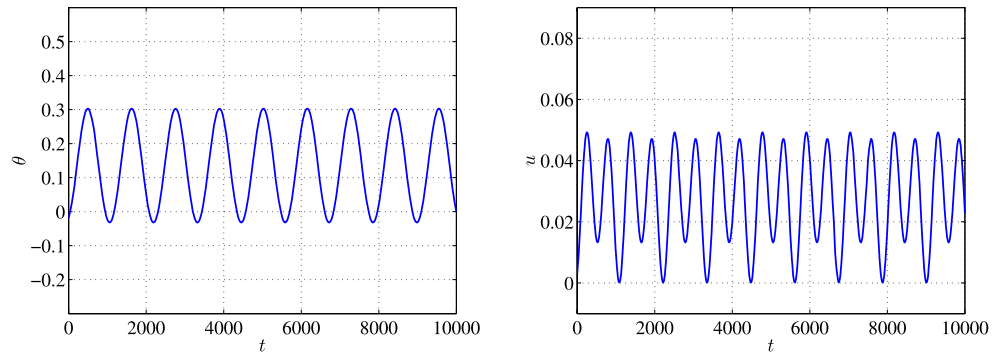

(a) $\sigma_1 = 0$ (b) $\sigma_1 = 0$

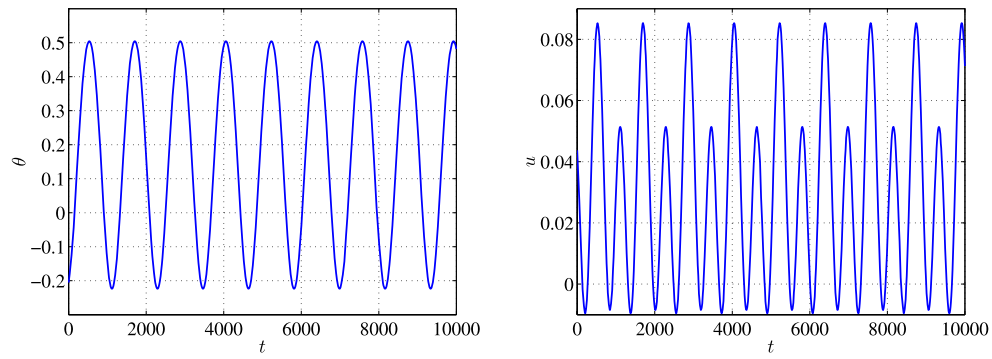

(c) $\sigma_1 = -0.0004$ (d) $\sigma_1 = -0.0004$

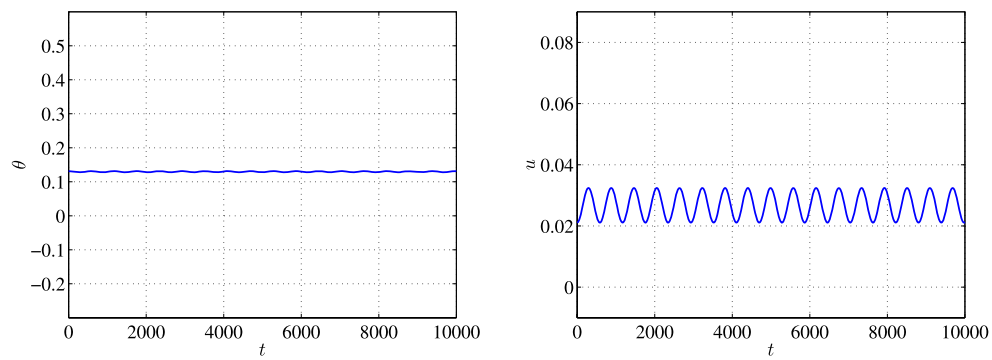

(e) $\sigma_1 = -0.0004$ (f) $\sigma_1 = -0.0004$

Fig. 10 Long-time histories of the micromirror response for $V_{\text{dc}} = 13.2$ V and $V_{\text{ac}} = 0.1$ V

The range where the internal resonance mechanism is active can be altered by changing the mirror natural frequencies which are functions of the torsional and bending stiffness of the suspension beams as well as the mass and moment of inertia of the micromirror. Further, for $V_{\text{dc}} \neq 0$, the size and location of the electrodes play an important role in determining the rates at which the natural frequencies decrease with DC voltage. Hence, they can also be utilized to vary the internal resonance point. The designer should note

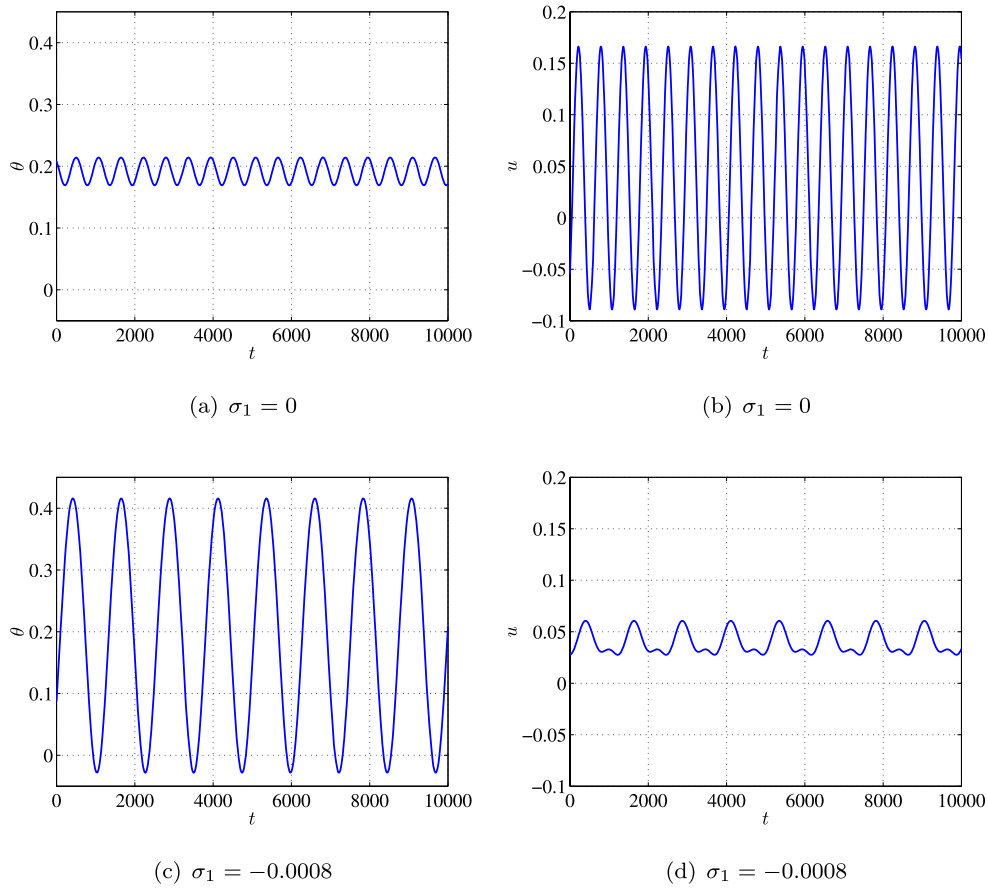

(a) $\sigma_1 = 0$ (b) $\sigma_1 = 0$

(c) $\sigma_1 = -0.0008$ (d) $\sigma_1 = -0.0008$

Fig. 11 Long-time histories of the micromirror response for $V_{\text{dc}} = 15$ V and $V_{\text{ac}} = 0.1$ V

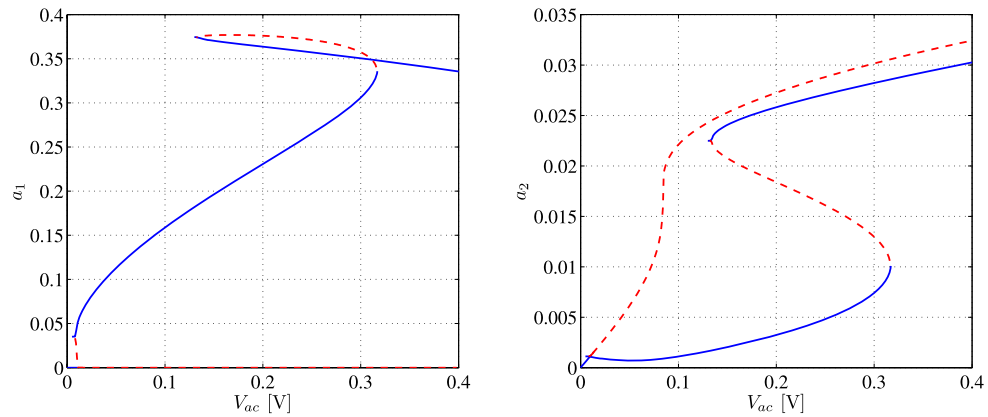

(a) (b)

Fig. 12 The force-response curves of the first and second modes when the second mode is excited near primary resonance $\sigma_1 = -0.00002$ and $V_{\text{dc}} = 13.2$ V

that, while for the mirror under consideration internal resonance occurred at a large DC voltage, slight variations in the mirror parameters can shift the internal resonance point towards smaller DC voltages, further limiting the operation range of the microscanner.

The simple design rule $\frac{\omega_2}{\omega_1} > 2.2$ at $V_{\text{dc}} = 0$, Fig. 3, can be used to eliminate the possibility of internal resonance between the first two modes over the whole scanner range of operation. One way to achieve that is to shorten the suspension beams. Since the torsional stiffness of the beam is inversely proportional to l while the bending stiffness is inversely proportional to l^3, the ratio $\frac{\omega_2}{\omega_1}$ is counter-proportional to l. Another approach is to increase the aspect ratio of the beam cross section $\frac{h}{w}$ while holding the section circumference $w + h$ constant. This significantly increases the second natural frequency while keeping the first natural frequency constant. These geometric design solutions can be combined with variations in the mass or dimensions of the rigid mirror plate. It is worth noting, however, that varying these parameters can increase the voltage requirement to realize the desired tilt angles. Consequently, it is important that these parameters are optimized to minimize additional voltage requirements. Further, it is important to keep in mind that avoiding the two-to-one internal resonance through increasing or decreasing the first two natural frequencies could as well activate higher-order internal resonances.

References

1. Van Kessel, P.F., Hornbeck, L.J., Meier, R.E., Douglass, M.R.: MEMS-based projection display. Proc. IEEE **86**(8), 1687–1704 (1998)
2. Ford, J.E., Aksyuk, V.A., Bishop, D.J., Walker, J.A.: Wavelength add-drop switching using tilting micromirrors. J. Lightwave Technol. **17**(5), 904–911 (1999)
3. Lin, L.Y., Goldstein, A.L., Tkach, R.W.: Free-space micromachined optical switches for optical networking. IEEE J. Sel. Top. Quantum Electron. **5**(1) (1999)
4. Collins, D.R., Sampsell, J.B., Hornbeck, L.J., Florence, P.A., Penz, P.A., Gately, M.T.: Application of improved deformable mirror array technology to neural network realization. Neural Netw. **1**(1), 378–382 (1988)
5. Cohn, R.W., Sampsell, J.B.: Deformable mirror device uses in frequency excision and optical switching. Appl. Opt. **27**, 937–940 (1988)
6. Hornbeck, L.J.: 128 multiplied by 128 deformable mirror device. IEEE Trans. Electron Dev. **30**(5), 539–545 (1983)
7. Fan, L., Yu, M.C.: Two-dimensional optical scanners with large angular rotation realized by self-assembled microelevator. In: Proceedings of the IEEE LEOS Summer Topical Meeting on Optical MEMS, Monterey, CA pp. 107–108 (1998)
8. Osterberg, P.M.: Electrostatically actuated microelectromechanical test structures for material property measurements. PhD thesis, MIT, Cambridge, MA (1995)
9. Hornbeck, L.J.: Deformable-mirror spatial light modulators. SPIE Crit. Rev. Ser. **1150**, 86–102 (1989)
10. Degani, O.B., Socher, E., Lipson, A., Leitner, T., Setter, D.J., Kaldor, S., Nemirovisky, Y.: Pull-in study of an electrostatic torsion microactuator. J. Microelectromech. Syst. **7**(4), 373–379 (1998)
11. Nemirovisky, Y., Degani, O.B.: A methodology and model for the pull-in parameters of electrostatic actuators. J. Microelectromech. Syst. **10**(4), 601–614 (2001)
12. Degani, O.B., Nemirovisky, Y.: Design considerations of rectangular electrostatic torsion actuators based on new analytical pull-in expressions. J. Microelectromech. Syst. **11**(1), 20–26 (2002)
13. Zhang, X.M., Chau, F.S., Quan, C., Liu, A.Q.: Modeling of the optical torsion micromirror. In: Proceedings of the SPIE Conference on Photonics Technology in the 21st Century: Semiconductors, Microstructures, and Nanostructures, Singapore, pp. 109–116 (1999)
14. Zhang, X.M., Chau, F.S., Quan, C., Lam, Y.L., Liu, A.Q.: Study of the static characteristics of a torsional micromirror. J. Microelectromech. Syst. **90**, 73–81 (2001)
15. Degani, O.B., Nemirovisky, Y.: Modeling the pull-in parameters of electrostatic actuators with a novel lumped two degrees of freedom pull-in model. Sens. Actuators A **97–98**, 569–578 (2002)
16. Huang, J.M., Liu, A.Q., Deng, Z.L., Zhang, Q.X., Ahn, J., Asundi, A.: An approach to the coupling effect between torsion and bending for electrostatic torsional micromirrors. Sens. Actuators A **115**, 159–167 (2004)
17. Wetzel, G.C., Strozewski, K.J.: Dynamical model of microscale electromechanical spatial light modulator. J. Appl. Phys. **73**(11), 7120–7124 (1993)
18. Sattler, R., Florian, P., Fattinger, G., Wachutka, G.: Modeling of an electrostatic torsional actuator: Demonstrated with an RF MEMS switch. Sens. Actuators A **97**, 337–346 (2002)
19. Sane, H.S., Yazdi, N., Carlos, H.M.: Application of sliding mode control to electrostatically actuated two-axis gimbaled micromirrors. In: Proceedings of the American Control Conference, Denver, CO, pp. 3726–3731 (2003)
20. Ataman, C., Urey, H.: Modeling and characterization of comb-actuated microscanners. J. Micromech. Microeng. **16**, 9–16 (2006)
21. Camon, H., Lanaudi, F.: Fabrication, simulation, and experiment of a rotating electrostatic silicon mirror with large angular deflections. In: Proceedings of the IEEE Micro Electro Mechanical Systems (MEMS), Japan, pp. 645–650 (2000)
22. Zhao, J.P., Chen, H.L., Huang, J.M., Liu, A.Q.: A study of dynamic characteristics and simulations of MEMS torsional micromirror. Sens. Actuators A **120**, 199–210 (2005)

23. Daqaq, M.F.: Adaptation of nontraditional control techniques to nonlinear micro and macro mechanical systems. PhD thesis, Virginia Tech, Blacksburg, VA (2006)
24. Timoshenko, S.: Theory of Plates and Shells. McGraw-Hill, New York (1987)
25. Nayfeh, A.H.: Introduction to Perturbation Techniques. Wiley-Interscience, New York (1981)
26. Daqaq, M.F., Abdel-Rahman, E.M., Nayfeh, A.H.: Towards a stable low-voltage torsional microscanner. Microsyst. Technol. **14**, 725–737 (2008)
27. Nayfeh, A.H.: Resolving controversies in the application of the method of multiple scales and the generalized method of averaging. Nonlinear Dyn. **40**, 61–102 (2005)
28. Arafat, H.N.: Nonlinear response of cantilever beams. PhD thesis, Virginia Tech, Blacksburg, VA (1999)